Effects of soot deposition on particle dynamics and microbial processes in marine surface waters

Xavier Mari, Jérôme Lefèvre, Jean-Pascal Torréton, Yvan Bettarel, Olivier
Pringault, Emma J. Rochelle-Newall, Patrick Marchesiello, Christophe E.
Menkès, Martine Rodier, Christophe Migon, et al.

HAL Id: hal-01139299
https://hal.science/hal-01139299

Submitted on 6 Apr 2021

Effects of soot deposition on particle dynamics and microbial processes in marine surface waters

Xavier Mari[1,2], Jérôme Lefèvre[3], Jean-Pascal Torréton[1], Yvan Bettarel[1], Olivier Pringault[1], Emma Rochelle-Newall[1,4], Patrick Marchesiello[3], Christophe Menkes[5], Martine Rodier[6], Christophe Migon[7,8], Chiaki Motegi[7,8], Markus G. Weinbauer[7,8], and Louis Legendre[7,8]

[1]IRD, UMR 5119 ECOSYM, Université Montpellier II, Montpellier, France, [2]Now at Aix-Marseille Université, Université de Toulon, CNRS/INSU, IRD, MIO, Marseille, France, [3]IRD, UMR 5566 LEGOS, Université de Toulouse, Toulouse, France, [4]Now at IRD, UMR 7618 IEES-Paris, Ecole Normale Supérieure, Paris, France, [5]IRD, UMR 7159 LOCEAN, Pierre et Marie Curie Université, Paris, France, [6]IRD, UMR 241 EIO, Centre IRD de Tahiti, Papeete, France, [7]Sorbonne Universités, UPMC, Université Paris 06, UMR 7093, LOV, Observatoire Océanologique, Villefranche-sur-Mer, France, [8]CNRS, UMR 7093, LOV, Observatoire Océanologique, Villefranche-sur-Mer, France

Abstract Large amounts of soot are continuously deposited on the global ocean. Even though significant concentrations of soot particles are found in marine waters, the effects of these aerosols on ocean ecosystems are currently unknown. Using a combination of in situ and experimental data, and results from an atmospheric transport model, we show that the deposition of soot particles from an oil-fired power plant impacted biogeochemical properties and the functioning of the pelagic ecosystem in tropical oligotrophic oceanic waters off New Caledonia. Deposition was followed by a major increase in the volume concentration of suspended particles, a change in the particle size spectra that resulted from a stimulation of aggregation processes, a 5% decrease in the concentration of dissolved organic carbon (DOC), a decreases of 33 and 23% in viral and free bacterial abundances, respectively, and a factor ~2 increase in the activity of particle-attached bacteria suggesting that soot introduced in the system favored bacterial growth. These patterns were confirmed by experiments with natural seawater conducted with both soot aerosols collected in the study area and standard diesel soot. The data suggest a strong impact of soot deposition on ocean surface particles, DOC, and microbial processes, at least near emission hot spots.

1. Introduction

Soot is emitted during the burning of biomass and combustion of fossil fuels. Because soot particles absorb solar radiation, high concentrations generate atmospheric brown clouds (ABCs) that generally occur over large cities and in specific regional hot spots [*Ramanathan et al.*, 2007; *Ramanathan and Carmichael*, 2008]. The effects of soot on atmospheric processes and climate have been intensively studied and well documented since the mid-1980s. In particular, it is now acknowledged that the magnitude of soot-related atmospheric warming may be equivalent to at least 50% that of CO_2 [*Chung et al.*, 2005; *Shindell and Faluvegi*, 2009], making soot the second largest contributor to the global warming observed during the twentieth century [*Jacobson*, 2002]. Unlike CO_2, the lifetime of soot particles in the atmosphere is short, i.e., it varies from a few days to several weeks depending on the aerosols' characteristics and atmospheric conditions [*Ogren and Charlson*, 1983; *Vignati et al.*, 2010]. Soot aerosols are removed from the atmosphere via dry or wet deposition on both land and the ocean. At the global scale, soot deposition on the ocean occurs at a rate of ~70 Tg C year^{-1} (which includes the organic and the elemental carbon fractions), with highest fluxes in the Northern Hemisphere and intertropical regions and wide regional heterogeneity [*Jurado et al.*, 2008]. Although soot aerosols can travel long distances and cross the oceans [*Hadley et al.*, 2007], most particles are preferentially deposited in the vicinity of emission sources [*Jurado et al.*, 2008] because of their short lifetime in the atmosphere. Soot aerosols can also be introduced in the sea and spread into marine systems via river runoff [*Mitra et al.*, 2002; *Dittmar et al.*, 2012]. In the water column, soot carbon (soot-C) was reported to account for 1 to 7% of dissolved organic carbon (DOC) [*Mannino and Harvey*, 2004; *Dittmar and Koch*, 2006; *Dittmar and Paeng*, 2009] and 1 to 20% of particulate organic carbon (POC) [*Flores-Cervantes et al.*, 2009]. In sediments soot-C can represent 10 to 35% of the total organic carbon [*Masiello and Druffel*, 1998; *Middelburg et al.*, 1999; *Lohmann et al.*, 2009].
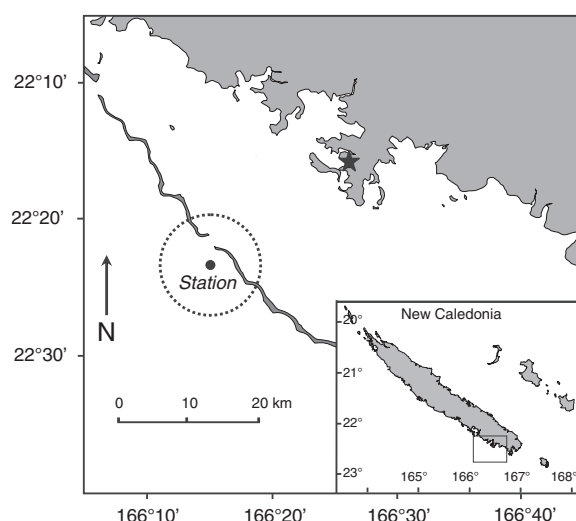
Figure 1. Map showing the location of the sampling station (black circle) in oceanic oligotrophic waters outside the barrier reef (22°24′35″S 166°14′35″E), the area of deposition of soot-like aerosols investigated (dashed circle of 10 km radius centered on the sampling station) used in Figure 3, and the position of the oil-fired power plant (black star) in Nouméa.

Owing to their high specific surface area-to-mass ratios (i.e., typically $>100\,m^2\,g^{-1}$) [*Koelmans et al.*, 2006], soot particles are highly surface active. It has been showed that soot particles efficiently adsorb organic matter in sediments [*Cornelissen et al.*, 2005; *Koelmans et al.*, 2006; *Lohmann et al.*, 2005]. In the water column, such high adsorptive properties of soot for organic matter could alter both the equilibrium between DOC and POC by stimulating the formation of transparent exopolymer particles (TEP) and the efficiency of aggregation. Recent studies have shown that microorganisms readily adsorb onto reference diesel soot particles [*Weinbauer et al.*, 2009; *Cattaneo et al.*, 2010]. Attachment of microorganisms to soot particles may enhance their removal from surface waters if these particles are consumed in situ or exported downward. Hence, soot particles can affect the functioning of the microbial food web and the ability of the pelagic ecosystem to export organic matter and cycle chemical elements. Despite the suspected effects of soot particles on marine pelagic processes, information on its dynamics in marine systems is scarce.

Our study investigates the effects of soot deposition on marine aggregates and microbial processes in surface waters and export fluxes downward. To achieve this, we monitored changes in physical, chemical, and biological variables during a major soot deposition event at an oligotrophic oceanic station off the barrier reef of the southwestern lagoon of New Caledonia. We also performed experiments on natural seawater, first with soot collected in the study area to assess the effect of soot on microbial activity and second with standard diesel soot to determine its effect on TEP formation.

2. Methods

2.1. Site

The island of New Caledonia is located in the oligotrophic tropical South Pacific Ocean, northeast of Australia. It is isolated from the influence of heavily industrialized areas and is not subjected to the strong deposition of anthropogenic aerosols that occurs mostly in the Northern Hemisphere [*Junker and Liousse*, 2006; *Jurado et al.*, 2008]. In addition, owing to the very low population density in New Caledonia, the production of soot by urban activity is probably low. There, the dominant and most regular source of atmospheric soot is the industrial oil-fired power plant located in the main city, Nouméa. According to the website of the Caledonian electricity company (Enercal), the fuel consumption of the oil-fired power plant on the industrial site of Doniambo is $165 \times 10^3\,kg\,h^{-1}$. Assuming an emission factor of 0.3 g of soot per kilogram of fuel consumed [*Bond et al.*, 2004], the power plant should emit approximately 50 kg soot h^{-1}. The transport of this anthropogenic soot is largely determined by meteorological conditions. During early summer, anticyclones migrate eastward in the subtropical belt, and they bring spells of moderate to strong southeasterly (SE) winds ($5–10\,m\,s^{-1}$) over New Caledonia, which last several days [*Lefèvre et al.*, 2010]. These conditions are sometimes interrupted by transient regimes during which the SE trade winds stop, allowing atmospheric brown clouds (ABCs) to stagnate over large areas surrounding the oil-fired power plant, which leads to deposition on the lands and waters under the ABCs.

The southwest lagoon of New Caledonia is an enclosed, relatively shallow coral lagoon surrounded by ultraoligotrophic oceanic waters. The coral barrier is located ~20 km from Nouméa (Figure 1), and it isolates the oceanic waters outside the barrier from the riverine inputs and urban effluents that are discharged

inside the lagoon [*Jouon et al.*, 2006]. The short-term input of soot particles coming from a well-identified source into ultraoligotrophic oceanic waters that are at other times under the influence of steady trade winds provides a unique opportunity for studying the short-term response of a sensitive oceanic pelagic system to soot deposition.

2.2. Sampling

Sampling was performed in the upper water column of a 700 m deep station located in the ocean outside the barrier reef (Figure 1). Samples were collected on 5 days between 10 and 19 November 2008. Temperature and salinity (conductivity-temperature-depth, CTD) profiles were recorded on each sampling day to determine the vertical density structure of the upper water column (0–20 m). Average temperature and salinity in the upper water column (0–20 m) were (mean ± standard deviation (SD)) 24.7 ± 0.4°C and 35.3 ± 0.1, respectively. Density gradients, $\Delta\rho/\Delta z$, were calculated for every 1 m interval from CTD casts. The vertical $\Delta\rho/\Delta z$ profiles showed that the physical characteristics of the water column remained constant during the sampling period, with no vertical stratification in the upper water column except very close to the surface (data not shown).

Model simulations of the seasonal cycle of surface ocean dynamics around New Caledonia indicate that near the sampling station, currents are westward and low (from 0.03 to 0.10 m s^{-1}) during typical November month due to the presence of trade winds [*Marchesiello et al.*, 2010]. Stopping of the trade winds may result in a strong diminution of these surface currents and, thus, increased retention time of deposited soot particles at the sampling station.

Particle size spectra were measured in situ from surface to bottom of the upper water column (0–20 m) (see below). Suspended particulate matter (SPM), chlorophyll *a* (chl *a*), dissolved organic carbon (DOC), and bacterial production (BP) were determined on seawater samples collected at 1 m depth using a Teflon air pump. After collection, the seawater samples were kept in 25 L polycarbonate carboys during transport to the laboratory (<2 h).

Soot deposited at the surface of the lagoon was collected in the Bay of Grande Rade (sampling position 22°15′49″S 166°26′24″E) for detailed chemical characterization. This was done at a distance of only 1 km from the oil-fired power plant (located beside the star that identifies the power plant in Figure 1) on one sampling occasion during a deposition event very localized in space that occurred on 26 June 2009. It was decided to take soot samples after observing the presence of a very large black slick at the surface of the water in the Bay adjacent to the power plant. Soot was collected by skimming the surface of the water with a 2 L polycarbonate bottle (the resulting sample was completely black). The soot suspension was transported to the laboratory and lyophilized for later analysis.

2.3. Atmospheric Simulations

The transport and deposition patterns of soot particles were determined using an atmospheric model simulation [*Lefèvre et al.*, 2010] in which we assumed that the oil-fired power plant located in Nouméa was the main source of soot. Atmospheric simulations were used to run a transport and dispersion model (FLEXPART-WRF) [*Fast and Easter*, 2006] and to predict the dry deposition of atmospheric soot released from the power plant during the sampling period. A density of 1.8 g cm^{-3} [*Choi et al.*, 1995] was used for soot particles. Considering that the size distribution of soot particles emitted by oil-fired power plants range from 50 nm to 5 μm or more in diameter [*Ahlberg et al.*, 1983], three deposition simulations were conducted assuming a size for soot particles of 50 nm, 500 nm, or 5 μm. Deposition of soot during the sampling period was calculated for a circular area of 10 km radius centered on the sampling station. Since other aerosols could present characteristics similar to those used in the model to represent soot particles (i.e., size range from 50 nm to 5 μm and density of 1.8 g cm^{-3}), we use the term "soot-like aerosols" for the results of the model simulations.

2.4. Particle Volume Concentration

Particle volume concentration profiles were measured in situ using a LISST-100X Type C (Laser In Situ Scattering and Transmissometry; Sequoia Scientific, Inc.) This equipment uses the technique of laser diffraction to obtain particles' equivalent spherical diameter (ESD; μm) and is calibrated by the manufacturer using microspheres of known sizes. Counts were automatically classified according to their ESD into 32 logarithmic size classes between 2.5 and 500 μm. The LISST-100X provides the volume of particles per size class and per unit volume of

water ($\mu m^3 \, mL^{-1}$). The data presented herein (particle volume expressed in μL instead of μm^3) were normalized to the width of each size class. Each value corresponds to the particle volume concentration ($\mu L \, L^{-1}$) measured by the LISST-100X at 1 m depth intervals.

2.5. Suspended Particulate Matter Concentrations

The dry weight of particles (SPM) was determined on duplicate 1 L samples filtered onto a preweighed 47 mm diameter 0.2 μm polycarbonate filter. After filtration, the filters were dried at 50°C for 24 h and weighed using a balance with ±0.001 mg precision.

2.6. Phytoplankton Biomass and Production

Concentrations of chl *a* were determined fluorometrically from 500 mL subsamples filtered onto 25 mm Whatman GF/F filters [*Holm-Hansen et al.*, 1965]. Particulate primary production (PP) was measured using $NaH^{14}CO_3$ [*Rochelle-Newall et al.*, 2008]. Water samples (63 mL) were inoculated with 0.74 MBq of $NaH^{14}CO_3$ (Perkin Elmer, initial concentration 37 $MBq \, mL^{-1}$) and immediately placed in a thermoregulated tank (22–24°C) exposed to daylight. For each sample, three replicates and one dark control were incubated for 5 h, typically from 08:00 to 13:00 or from 13:00 to 18:00. After incubation, the samples were gently filtered onto 0.4 μm polycarbonate filters (Whatman Cyclopore). After acidification with 100 μL of 0.5 N HCl and drying (12 h at 45°C), the filters were placed in scintillation vials with 5 mL of scintillation cocktail (Ultima Gold MV, Packard instruments) and counted using a Packard Tri-Carb (1600TR) Liquid Scintillation Counter. Counting efficiency was determined by external standards. The amount of ^{14}C incorporated was computed using an inorganic carbon concentration of 25,700 $\mu g \, C \, L^{-1}$ [*Marañón et al.*, 2004].

2.7. Dissolved Organic Carbon Concentrations

Analyses of DOC were performed on 10 mL subsamples filtered through 47 mm precombusted Whatman GF/F filters and collected in precombusted (450°C, 12 h) 10 mL glass ampoules, preserved with 12 μL of 85% phosphoric acid (H_3PO_4). Samples were stored in the dark until analysis. The DOC concentration was measured on a Shimadzu total organic carbon (TOC) VCPH analyzer. A calibration curve was constructed for each sample run using five known concentrations that covered the expected sample range. In this case it was 0 to 500 $\mu mol \, C \, L^{-1}$, made up using potassium phthalate, the commonly used DOC standard. Certified reference materials (low carbon water and deep seawater standards from the Hansell Laboratory, University of Miami) were used as external standards to assess the performance of the instrument on and between measurement days and to determine the machine blank. Both the low carbon water (2 $\mu mol \, C \, L^{-1}$) and the deep seawater standard (44 $\mu mol \, C \, L^{-1}$) were used at the beginning and at the end of each sample run (analysis day). This allowed us to accurately assess the machine variability not only between days but also during a sample run. Within each sample run, there was very little variation of the machine blank (1–1.5 $\mu mol \, C \, L^{-1}$; CV $< 2\%$). Milli-Q blanks were regularly injected as "sample blanks" during the analysis sequence to ensure that no sample carry over was observed. The machine blank was between 3 and 5 $\mu mol \, C \, L^{-1}$ on the measurement days. The reported values are blank corrected.

2.8. Abundances of Free Bacteria and Viruses

Duplicate subsamples of 500 μL were fixed immediately after collection with 0.02 μm filtered glutaraldehyde (final concentration 1% [vol:vol]) and analyzed the same day. Samples were filtered (vacuum < 15 kPa) through 0.02 μm pore size Anodisc membrane filters (Whatman, Maidstone, UK). Free bacterial cells and viruses were counted under a Leitz Laborlux D epifluorescence microscope after staining the membranes with SYBR Gold (Molecular Probes Europe, Leiden, Netherlands) for 15 min in the dark [*Chen et al.*, 2001].

2.9. Bulk and Particle-Attached ($>1 \, \mu m$) Bacterial Production, Bacterial Respiration, and Bacterial Growth Efficiency

Duplicate 5 mL subsamples received L-[3,4,5-^{3}H]-Leucine (40 $nmol \, L^{-1}$ final concentration, PerkinElmer, 4 $TBq \, mmol^{-1}$). After 60 min in the dark at in situ temperature, incorporation was stopped with glutaraldehyde (2% final concentration), and 1.5 mL subsamples were distributed into 2 mL centrifuge tubes and further processed [*Smith and Azam*, 1992] to estimate bulk incorporation. The remaining 3.5 mL were filtered (vacuum < 7 kPa) onto 1 μm porosity Nuclepore filters for attached production and rinsed with 0.2 μm of filtered seawater. After disconnection of the vacuum, the filters received 15 mL of 5% trichloroacetic acid (TCA), the macromolecules were allowed to precipitate for 15 min at 4°C, and the filters were rinsed 3 times
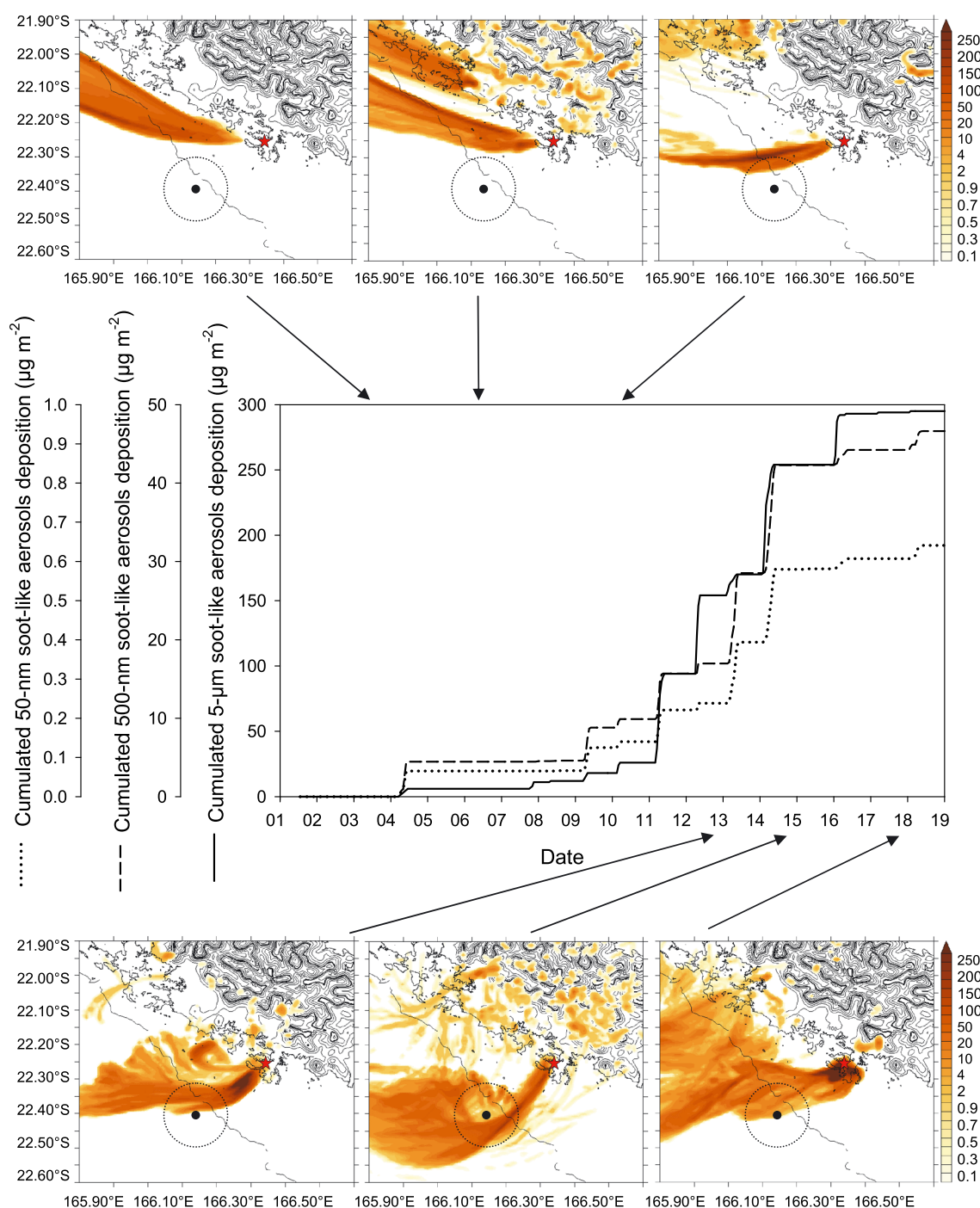
Figure 2. Examples of the areas impacted by dry deposition of soot-like aerosols from the Nouméa oil-fired power plant. The six maps illustrate the results of runs with soot-like particles of 500 nm in size, integrated from 00:00 to 08:00 (ship sampling was at 08:00 on each day) as modeled from 10 to 19 November 2008. The graph shows the cumulated deposition of soot-like particles of 50 nm, 500 nm, and 5 μm diameter over the sampling period. The dry deposition of aerosols (μg) is given per unit mass of aerosols emitted (metric ton) and per unit area (m^2).

with cold 5% TCA. A glutaraldehyde-killed blank was used for each duplicate and treated as above. Following the addition of scintillation cocktail (Ultima Gold MV), radioactivity was determined with a Packard LTR1600 LSC after quenching correction using external standards. Duplicates differed on average by 2 and 5% for bulk and >1 μm BP, respectively. Regular checks showed that ^{3}H-Leu incorporation
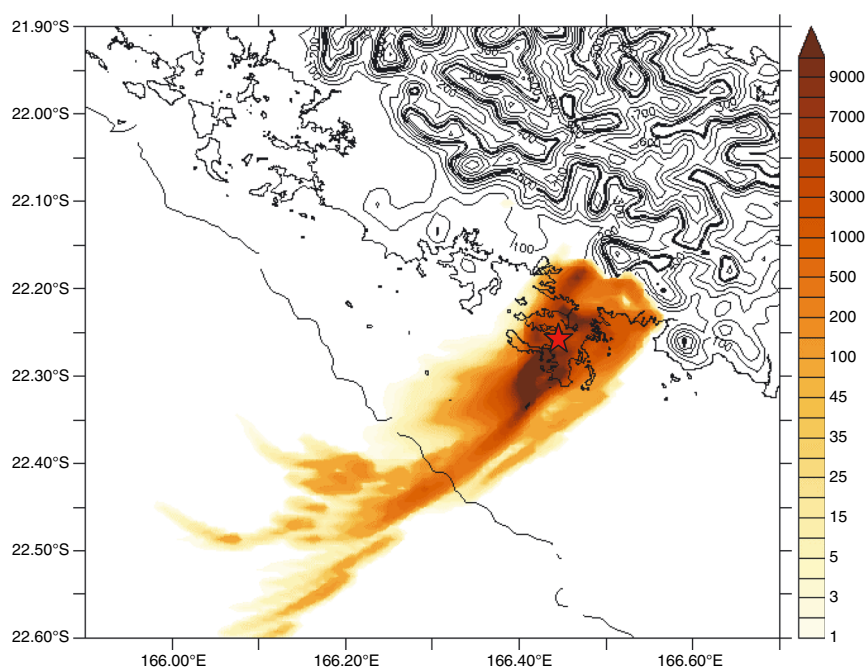
Figure 3. Modeled area of deposition of soot-like aerosols (the figure illustrates the results of runs with soot-like particles of 5 μm in size) during the localized deposition event that occurred on 26 June 2009, integrated from 00:00 to 08:00 (ship sampling was at 08:00). The dry deposition of aerosols (μg) is given per unit mass of aerosols emitted (metric ton) and per unit area (m^2).

reached a plateau well below 40 nmol L^{-1} and was linear during the 60 min incubations. Bacterial respiration (BR) and bacterial growth efficiency (BGE) were calculated from average BP values using an empirical model [*del Giorgio and Cole*, 1998].

2.10. Experiment on the Effect of Soot on Bacterial Activity

A short-term experiment that aimed at determining the effect of soot deposition on bacterial activity was conducted in June 2009 by incubating seawater collected at the sampling station in two carboys, one without (control) and the other with soot enrichment (treatment, see below), during 29 h. Each carboy received 20 L of seawater. The soot material used in this experiment had been collected using Continuous Ambient Particulate tapered element oscillating microbalance (TEOM) Monitors (Thermo Scientific TEOM 1400ab) installed in the vicinity of the Nouméa oil-fired power plant. This type of equipment provides a continuous

Table 1. Variations in the In Situ Characteristics at the Sampling Station at 1 m Depth Between 10 and 19 November 2008[a]

	10 November	12 November	14 November	17 November	19 November
BP (μg C L^{-1} h^{-1})	0.05 ± 0.00	0.04 ± 0.00	0.05 ± 0.00	0.06 ± 0.00	0.12 ± 0.00
%BP > 1 μm	14.5 ± 1.2	30.8 ± 1.2	13.2 ± 0.6	20.6 ± 0.8	28.8 ± 2.5
BR (μg C L^{-1} h^{-1})	1.05 ± 0.02	1.02 ± 0.01	1.03 ± 0.02	1.13 ± 0.01	1.54 ± 0.00
BGE (%)	3.62 ± 0.07	3.51 ± 0.02	3.58 ± 0.00	3.92 ± 0.00	5.92 ± 0.00
Particle volume concentration (μL L^{-1})	1.1	32.1	41.1	21.8	10.9
SPM (mg L^{-1})	0.10 ± 0.00	0.55 ± 0.07	0.45 ± 0.21	0.25 ± 0.07	0.40 ± 0.14
Chl *a* (μg L^{-1})	0.098	0.083	0.108	0.105	0.254
DOC (μmol L^{-1})	70.7 ± 0.3	70.6 ± 0.8	66.9 ± 0.8	69.1 ± 0.6	69.0 ± 0.9
Free bacteria (10^3 mL^{-1})	620 ± 50	600 ± 80	480 ± 40	480 ± 10	600 ± 40
Viruses (10^6 mL^{-1})	6.6 ± 0.9	4.7 ± 0.8	4.4 ± 0.3	5.9 ± 0.7	5.0 ± 0.2

[a]Bulk and particle-attached (>1 μm) bacterial production (BP): averages (±SD) of two measurements obtained by ^{3}H-leucine incorporation into cold trichloroacetic acid (TCA)-insoluble material. Bacterial respiration (BR) and bacterial growth efficiency (BGE): computed from average BP values. Particle volume concentration: measured in situ with the LISST-100X at 1 m depth. Suspended particulate matter concentrations (SPM): averages (±SD) of two measurements. Chlorophyll a (Chl *a*): single measurements on 500 mL subsamples. Dissolved organic carbon concentrations (DOC): averages (±SD) of six measurements (three injections from duplicate samples). Bacterial and viral abundances: averages (±SD) of two measurements.
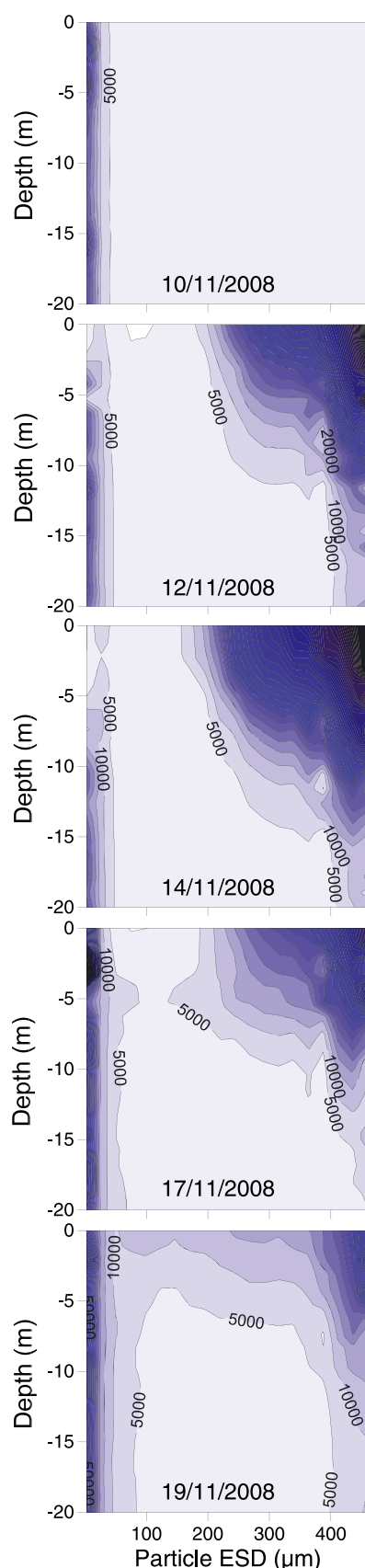
direct mass measurement of atmospheric suspended particles <10 μm utilizing a tapered element oscillating microbalance (TEOM); it is used for air quality monitoring in Nouméa by the Caledonian Association of Air Quality (Scalair).

A total of 15 TOEM filters provided by Scalair were placed in Milli-Q water and sonicated for 15 min in order to detach aerosols from filters. The blackish solution obtained after sonication was used to enrich the soot treatment. The concentration of carbon added, determined from the difference in total organic carbon (TOC) measured at T_0 in the treatment (i.e., 80.4 ± 1.6 μmol C L^{-1}) and in the control (73.0 ± 1.1 μmol C L^{-1}), was 7.4 μmol C L^{-1}. Considering that the specific carbon content of industrial soot ranges between 10 and 40% of the mass [*Liousse et al.*, 1996; *Dachs and Eisenreich*, 2000], the observed C enrichment corresponded to an addition of 225–900 μg soot L^{-1} (i.e., soot addition per liter of seawater sample). Incubations were conducted without agitation in a thermoregulated tank (22–24°C) exposed to daylight. Bacterial and primary production was determined in the control and in the treatment 6 and 4 times, respectively, during the 29 h incubation. The concentration of DOC was measured at the beginning and at the end of the experiment.

2.11. Experiment on the Effect of Soot on Formation of Transparent Exopolymer Particles

The effect of soot particles on TEP formation was studied in the laboratory by monitoring the size spectra of TEP formed from dissolved organic matter under controlled turbulence conditions in two 2 L Plexiglas containers, one without (control) and the other with soot enrichment (treatment). The soot material used in this experiment was reference diesel particulate matter (SRM2975; National Institute of Standards and Technology). Standard diesel soot was added to the treatment to reach a concentration of 10 μg mL^{-1}. Bulk seawater collected in the lagoon of New Caledonia in June 2009 was immediately filtered under low and constant vacuum pressure (<15 kPa) through 47 mm diameter GF/C Whatman filters (nominal pore size of 1.2 μm) in order to remove particles, including large TEP. The filtrate (2 L), which contained submicrometer TEP precursors, was put inside a mixing device [*Mari and Robert*, 2008]. This device, composed of two grids oscillating vertically inside two 2 L cylindrical containers, generates small-scale turbulence. The formation of TEP aggregates was monitored at room temperature (approximately 22°C) under increasing turbulence intensities, tuned at the start of three successive 1 h periods. The turbulence kinetic energy dissipation rate, ε, was set to 0.1, 1, and 10 cm^2 s^{-3}, during the first, second, and third hour of the experiment, respectively, by adjusting the frequency of oscillation of the grids. Samples were collected every 15 min (i.e., 13 sampling occasions during the 3 h

Figure 4. Vertical distributions of in situ volume concentration of particles (μm^3 mL^{-1} μm^{-1}) as a function of their equivalent spherical diameter (ESD; μm) in the upper water column (0–20 m) from 10 to 19 November 2008, determined using a submersible laser particle size analyzer (LISST-100X).
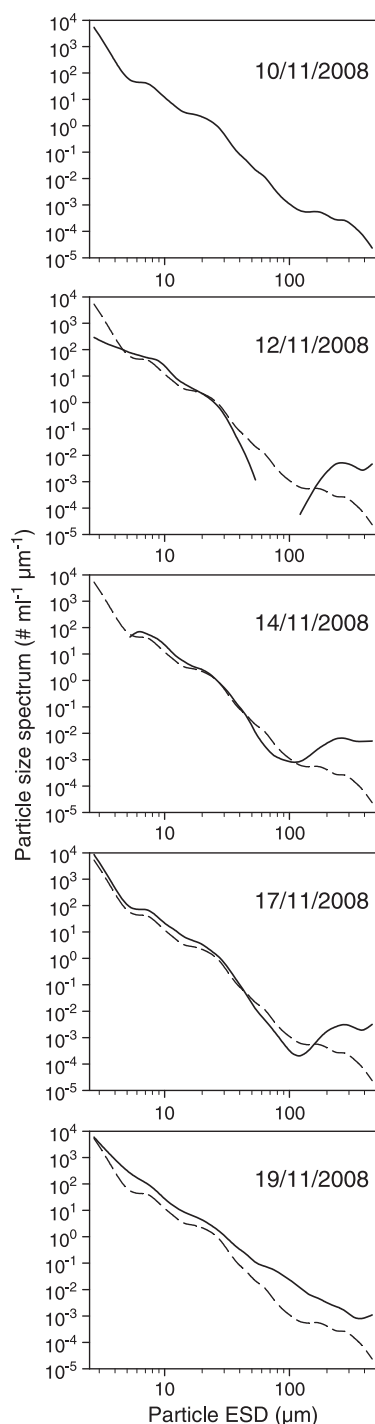
Figure 5. Size spectra of particles (mL^{-1} μm^{-1}) as a function of their equivalent spherical diameter (ESD; μm) at a 1 m depth measured in situ on five sampling days from 10 to 19 November 2008. The dashed lines represent the size spectra observed on 10 November, as visual reference. The missing parts of the spectra on 12 and 14 November (particles between 50 and 150 μm and 2.5 and 5 μm, respectively) are discussed in the text.

experiment) in both the control and the treatment to determine TEP size spectra.

The TEP size spectra were determined from 5 ml subsamples filtered onto 0.2 μm polycarbonate filters, stained with Alcian blue, after transferring the retained particles onto a microscope slide [*Passow and Alldredge*, 1994]. For each slide, 10 pictures were taken at two successive magnifications (250X and 400X) using a compound light microscope. The equivalent spherical diameter (ESD; μm) of individual TEP was calculated by measuring its cross-sectional area with an image-analysis system (Image-Pro Plus 7.0, Media Cybernetics), and counts were combined and classified into 20 logarithmic size classes [*Mari and Burd*, 1998]. The TEP volume concentration was calculated from the TEP size spectra assuming a spherical volume for each particle. The TEP carbon concentration (TEP-C; μg C mL^{-1}) was estimated by combining TEP size spectra with the relationship providing the carbon content of a given TEP particle according to its size [*Mari*, 1999]. The concentration of DOC was measured in the control and in the treatment at T_0, i.e., after addition of soot to the treatment.

2.12. Chemical Characterization of Soot

Soot collected at the water surface in the Bay of Grande Rade during the deposition event that occurred on 26 June 2009 was analyzed for elemental carbon (EC), total carbon (TC), and total nitrogen (TN). Lyophilized aerosols were placed on precombusted 25 mm diameter GF/F filters. Ten filters were prepared for EC and TC analysis, respectively, by weighing progressively increasing masses of lyophilized aerosols onto the filters (from 0.4 to 6.6 mg). For EC analyses, filters underwent a chemothermal oxidation (CTO) pretreatment at $340 \pm 0.5°C$ for 2 h to remove organic carbon and under an oxidative gas flow to prevent charring during the treatment [*Cachier et al.*, 1989; *Kuhlbusch*, 1995]. According to *Nguyen et al.* [2004], this CTO in oxygen at 340°C yields similar results for soot than CTO in air at 375°C [*Gustafsson et al.*, 1997]. After CTO, the filters were acidified with 100 μL of 0.5 N H_2SO_4 and then dried at 60°C in order to remove inorganic carbon. Particulate carbon and nitrogen were determined by high-temperature combustion (900°C) performed on a CN Integra mass spectrometer [*Raimbault et al.*, 2008]. The concentrations of EC, TC, and TN were calculated as the slopes of the regression lines of elemental particulate carbon (EC; μg C $filter^{-1}$), total particulate carbon (TC; μg C $filter^{-1}$), and total particulate nitrogen (TN; μg N $filter^{-1}$) on the mass of lyophilized aerosols (LA; μg). The C:N molar ratio was calculated as the ratio between the slopes of the regression lines of TC (μg C $filter^{-1}$) on LA (μg) and of TN (μg N $filter^{-1}$) on LA (μg).

3. Results

3.1. Soot Deposition and Elemental Carbon Composition

The first sampling day (10 November 2008) was characterized by moderate trade winds (4 m s^{-1}) that kept the atmospheric soot-like aerosols produced by the power plant in Nouméa
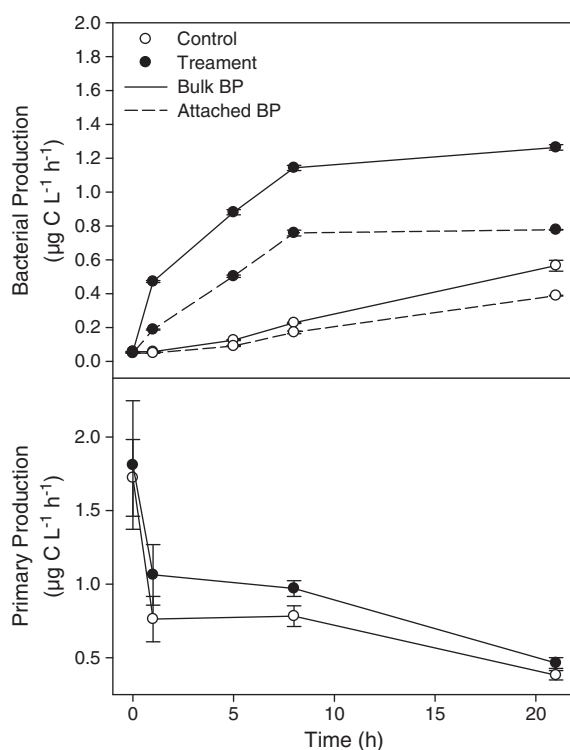
Figure 6. Bulk and attached bacterial production and primary production during the carboy incubation experiment in the control and soot-enriched samples. Each value is the average (±SD) of two measurements for BP and of three measurements for PP.

away from the sampling station. Such conditions are dominant most of the year. The trade winds relaxed on 11 November, leading to the formation of a large ABC over most of the lagoon that lasted for a few days. Between the first and second sampling days (10 and 12 November 2008), we visually observed the formation of a large ABC over most of the SW lagoon. The numerical transport and deposition model of soot-like aerosols reproduced this pattern and confirmed that aerosols from the power plant were deposited near the sampling station during the period of trade winds relaxation (Figure 2). Even if the simulated amount of soot-like aerosols deposited in the studied area varied greatly according to hypothesized particle sizes, i.e., 0.40, 28, and 71 $\mu g\,m^{-2}$ for soot-like aerosols of 50 nm, 500 nm, and 5 μm diameter, respectively, there was massive deposition for the three particle sizes between 11 and 14 November.

The numerical model also illustrated the strong deposition of soot-like aerosols that occurred on 26 June 2009 (Figure 3). The material collected at the sea surface on that date was composed of 8.9% EC per dry weight (EC = 0.089 LA + 0.142; $n = 10$; $r^2 = 0.97$), 15.0% TC per dry weight (TC = 0.150 LA + 0.131; $n = 10$; $r^2 = 0.97$), and 0.4% TN per dry weight (TN = 4.4×10^{-3} LA + 3.4×10^{-3}; $n = 10$; $r^2 = 0.99$), yielding a EC:TC ratio of 0.59 and a C:N molar ratio of 29.

3.2. Changes in Particle Size Spectra and Dissolved Organic Carbon Concentration at Sea

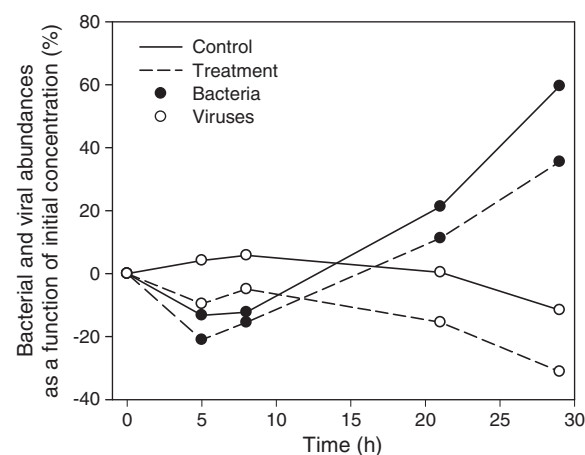On 10 November, the total volume concentration of particles in the water column was low and constant over the upper 20 m, where it averaged (±SD) $1.1 \pm 0.1\,\mu L\,L^{-1}$ ($1.1\,\mu L\,L^{-1}$ at 1 m depth; Table 1). On 12 November, the situation changed drastically, and the volume concentration in surface waters (1 m depth) increased by a factor of approximately 30 (and by up to 40 on 14 November). From that date onward, the volume concentration of particles decreased progressively with increasing depth, the values at depths >10 m being similar to those observed on 10 November (Figure 4). Large particles (>200 μm ESD) appeared in surface waters after 10 November but were never detected below 10 m depth. Along with the observed increase in the total volume of particles after 10 November, SPM at 1 m depth also increased by a factor of 5.5 (i.e., by 0.45 $\mu g\,L^{-1}$; Table 1), but this increase represented an enrichment factor

Figure 7. Variations of abundances of bacteria and viruses during the carboy incubation experiment in the control and soot-enriched samples, as a function of initial concentrations.
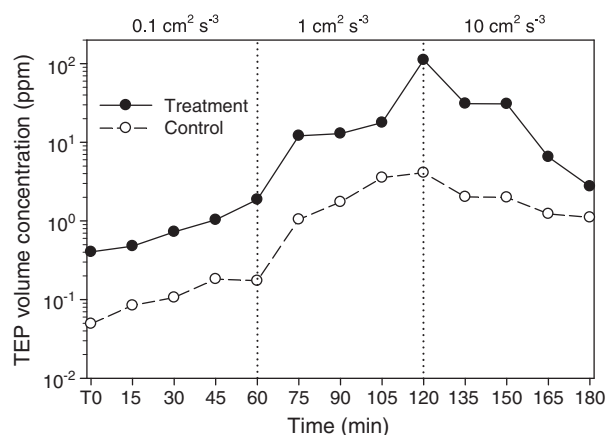
Figure 8. Volume concentration of TEP formed in the control and in the treatment during the experiment with three increasingly turbulent conditions. The vertical dashed lines represent the passage from one turbulence level to the next.

1 order of magnitude lower than the corresponding increase in particle volume concentration.

On 10 November, a typical steady state power law size spectrum was observed for particles in surface waters (Figure 5). This pattern changed radically after the deposition of soot-like aerosols (according to the atmospheric transport and deposition model), as the particle size spectra became bimodal from 12 to 17 November, thus deviating greatly from the power law relationship observed on 10 November. The bimodal size spectra were characterized by an increase in the concentration of particles >200 µm and a drastic decrease in the concentration of particles 2.5–5 and 50–150 µm (Figure 5).

Simultaneously, a significant decrease in DOC (t test on difference between means on the two dates; $p < 0.005$) occurred from 10 to 14 November of >5% (i.e., 3.8 µmol C L^{-1}; Table 1).

3.3. Changes in Microbial Biomass and Processes at Sea

The deposition of soot-like aerosols (according to the atmospheric transport and deposition model) was followed by significant changes in microbial processes in the water column. Concomitant with the changes described above, the in situ abundances of viruses and free bacteria decreased by 33% and 23%, respectively, between 10 and 14 November, before rising back to initial levels (Table 1). The decrease in viral abundance (mL^{-1}) was significantly related to the increases in both SPM concentration (µg L^{-1}) (i.e., [Virus] = $-4,880$ [SPM] + 7,028,000; $n = 5$; $r^2 = 0.90$; and $p = 0.014$) and particle volume concentration (Part$_{vol}$; µg L^{-1}) (i.e., [Virus] = $-46,030$ [Part$_{vol}$] + 6,305,000; $n = 5$; $r^2 = 0.66$; and $p = 0.096$). The decrease in abundances of free bacteria was not related to the increase in SPM concentration ($r^2 = 0.01$) but instead to the increase in particle volume concentration (i.e., [Bacteria] = $-2,749$ [Part$_{vol}$] + 614,809; $n = 5$; $r^2 = 0.40$; and $p = 0.255$).

The increase in volume concentration of particles between 10 and 12 November coincided with a twofold increase in the particle-attached fraction of bacterial production (%BP > 1 µm), and a few days after deposition of soot-like aerosols (according to the atmospheric transport and deposition model), bulk BP increased by a factor of 3 (Table 1). Concomitantly, BR increased by 50%, and BGE increased by a factor of 2 (Table 1). The increase in %BP > 1 µm was not proportional to the increase in particle volume concentration but followed instead the increase in SPM
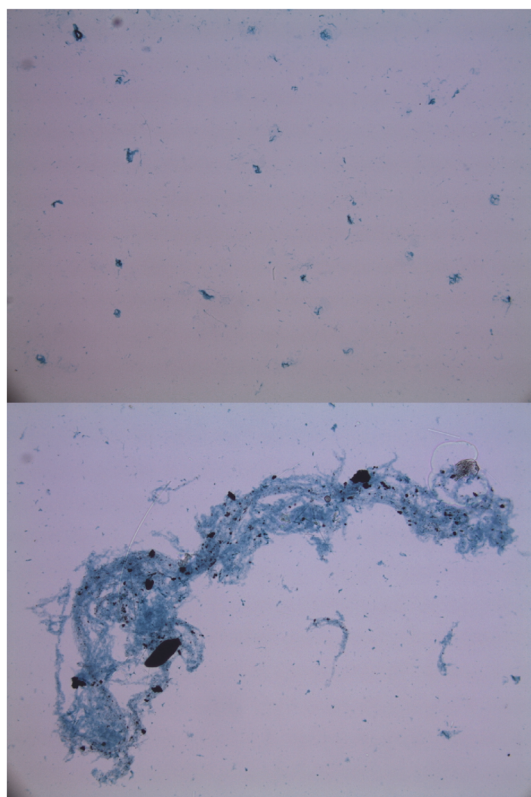

Figure 9. Examples of TEP observed in (top) the control and (bottom) the treatment at T_{120}. The black inclusions in the large TEP are soot particles.
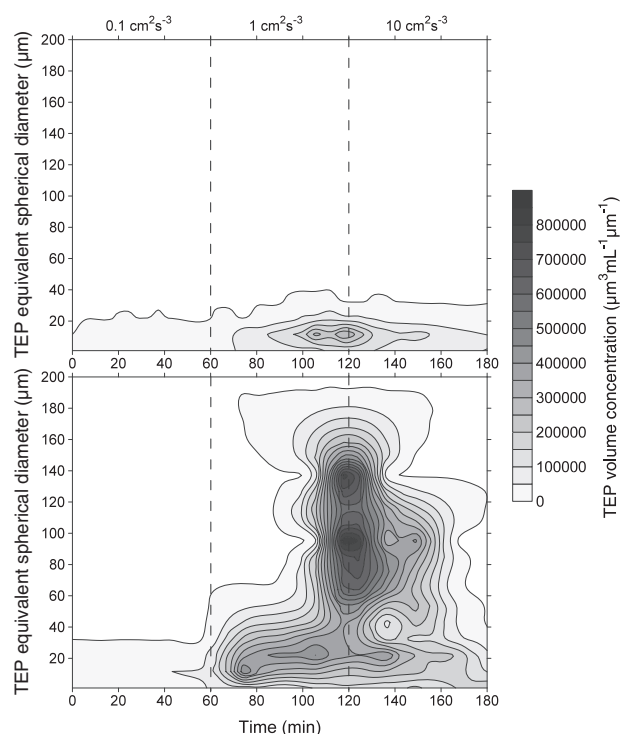
Figure 10. TEP volume concentration per size class of TEP formed in (top) the control and in (bottom) the treatment during the experiment with three increasingly turbulent conditions. The vertical dashed lines represent the passage from one turbulence level to the next.

concentration (Table 1). The chl a concentration remained constant during 1 week after the start of the deposition event of soot-like aerosols, before increasing by 160% on 19 November (Table 1).

3.4. Effects of Soot on Microbial Processes in the Laboratory

The effects of soot addition on bacterial activity were assessed in a carboy experiment where seawater was enriched with soot from the Nouméa power plant and incubated during 29 h. Bulk BP in the soot-enriched treatment was 8.2, 7.0, 5.0, 2.2, and 1.4 times higher than in the control after 1, 5, 8, 21, and 29 h of incubation, respectively. In addition and similar to the in situ observation, % BP > 1 μm was stimulated in the soot-enriched carboy (Figure 6). During the course of the experiment, there were no significant differences in PP between the soot treatment and the control (Figure 6), which agreed with the field observation that the deposition of soot did not enhance chl

a concentrations on the short term. The observed increase in BP was more than twice as large as the corresponding increase in BR, which resulted in an increase of bacterial growth efficiency.

At the start of the experiment, the DOC concentration was 63.2 and 71.2 μmol C L^{-1} in the control and the soot treatment, respectively. The higher concentration of DOC in the soot treatment is likely due to the input of soot-C in the dissolved phase. At the end of the experiment, the DOC concentration was 71.1 and 73.8 μmol C L^{-1} in the control and the soot treatment, respectively, thus corresponding to an absolute difference of 2.7 μmol C L^{-1}. Considering the changes of DOC concentration during the experiment, DOC increased by 7.9 and 2.5 μmol C L^{-1} in the control and the treatment, respectively, i.e., DOC increase in the treatment was 5.4 μmol C L^{-1} lower than in the control. Abundances of free bacteria and viruses were always lower in the soot-enriched treatment than in the control (Figure 7) with, on average, 11 and 15% less bacteria and viruses, respectively.

3.5. Effect of Soot on TEP Formation From Dissolved Organic Matter in the Laboratory

The effects of soot addition on TEP formation from dissolved organic matter were assessed in a laboratory experiment where seawater was enriched with standard diesel soot and incubated in a mixing device during 3 h. In the treatment, the TEP volume concentration increased immediately after soot enrichment and remained 1 order of magnitude higher than in the control during the course of the experiment (Figure 8). Changes in spectral TEP volume concentration showed that the buildup of the excess TEP pool in the treatment was mostly due to an increase concentration of large TEP (>30 μm equivalent spherical diameter, Figures 9 and 10). The volume concentration of TEP in the control and the treatment increased regularly at low and medium turbulence levels (from T_0 to T_{120}) and decreased abruptly at high turbulence level (from T_{120} to T_{180}) corresponding to disaggregation of large TEP. Comparison of treatment and control shows that the soot-induced formation of large TEP resulted in the production of excess TEP-C concentration in the treatment of 0.96 μmol C L^{-1} immediately after soot addition (i.e., without the effect of turbulence) to 96.95 μmol C L^{-1} after 1 h under an energy dissipation rate of 1 cm^2 s^{-3} (i.e., at T_{120}). Considering that 10 μg

soot mL^{-1} were added in the treatment, the excess TEP formation ranged between 0.096 and 9.695 µmol of TEP-C per milligram of soot added, at T_0 and T_{120}, respectively. In addition, there was a decrease of DOC concentration by 6.36 µmol C L^{-1} (i.e., diminution of 8% in comparison with the control) immediately after soot enrichment. This observed DOC removal supports the idea that the soot-induced TEP formation was fueled by the DOC pool. However, the instantaneous diminution of DOC concentration subsequent to soot addition was higher than the simultaneous increase in TEP-C concentration (i.e., 0.96 µmol C L^{-1}). This discrepancy between the DOC removed and the TEP-C produced may be due to a stimulation of DOC adsorption by the soot particles retained on the GF/F filters used to prepared DOC samples prior measurement and/or to an underestimation of TEP-C concentration obtained from the TEP size spectra using the relationship providing the carbon content of a given TEP particle according to its size.

4. Discussion

4.1. Soot Deposition

Given that the EC:TC ratio of reference diesel soot is ~0.78 [*Gustafsson et al.*, 2001], the high EC:TC ratio of the material collected at the sea surface in the Bay of Grande Rade on 26 June 2009 (i.e., 0.59) indicates that the material deposited at the lagoon surface near the oil-fired power plant had a strong chemical signature of soot. In addition, since diesel soot has a C:N molar ratio of 38 [*Song and Peng*, 2010], the high C:N molar ratio (i.e., 29) of the material collected in June 2009 strengthens this conclusion. Hence, a significant fraction of the aerosols produced by the Noumea oil-fired power plant and deposited on the lagoon was likely soot.

4.2. Vertical Dynamics of Particles

After deposition of soot-like aerosols (according to the atmospheric transport and deposition model), the volume concentration of particles (measured in situ with the LISST instrument) increased dramatically in surface waters, due to the appearance of very large particles (>200 µm). However, the buildup of this large particulate pool was only observed in the upper 10 m. At depths >10 m, the volume concentration of particles was similar to the values in the surface layer before the deposition event. This vertical pattern indicates that the observed increase in volume concentration resulted from an input of particles at the sea surface. The lack of increase in particle volume concentration below 10 m suggests that either the large particles generated after deposition of soot-like aerosols had almost neutral buoyancy and settled very slowly and/or their continuing aggregation during settling produced particles that were larger than the maximum size that could be detected with our equipment (i.e., 500 µm). While no sediment trap data are available that could be used to test these two ideas, the high density of soot particles (approximately 1.8 g cm^{-3}) [*Choi et al.*, 1995] supports the idea of a soot-enhanced downward export via formation of large soot-ballasted fast-sinking aggregates. Actually, the rapid sinking of large (>200 µm ESD) soot-ballasted aggregates may be responsible for the reduction (even disappearance on 12 November) of particle concentrations in the 50–150 µm size range via enhanced aggregation by differential sedimentation. In other words, these large fast-sinking aggregates may act as sinking nets trapping particles of specific sizes during their journey to the deep.

4.3. Aggregation Linked to Soot Adsorptive Properties

Both the in situ observations and the TEP formation experiment showed that the input of soot was followed by changes in particle aggregation processes. Subsequent to deposition of soot-like aerosols at sea (according to the atmospheric transport and deposition model), the volume of particles in the surface layer increased by a factor of 30 to 40, while the concentration of SPM increased by a factor of 5.5. The two increases likely reflect the input of soot to the marine system, and their differences in amplitudes can be explained by two mechanisms. First, because aggregation creates fractal particles, the apparent volume of an aggregate is much larger than the sum of the volumes of the units composing it. In other words, during aggregation and the buildup of fractal aggregates, volume growth does scale with particle porosity and not with the increased mass due to the input of aerosols. Second, soot is composed of surface active particles that may adsorb organic material very efficiently, thus transferring small-sized organic matter that is not detected by the LISST (i.e., <2.5 µm) to larger-sized particles. Therefore, the observed increase in particle volume concentration may partly be explained by the up-size transfer of small organic particles (<2.5 µm) that were

already taken into account in SPM measurements before aerosols deposition. The latter mechanism is supported by the observed decrease in both concentrations of DOC and abundances of free bacteria and viruses that occurred after deposition, assuming that both DOC and small particles were adsorbed on soot particles.

Our interpretation of the above observations as a stimulation of aggregation (termed overaggregation) by the deposited aerosols is supported by the peculiar shape of the in situ particle size spectrum observed subsequent to deposition of soot-like aerosols, which deviated greatly from the observed typical predeposition power law relationship. Deviation from the steady state size distribution may occur as a result of alteration of coagulation processes [*McCave*, 1984]. The drastic reduction (even disappearance) of small particle concentrations in the 2.5–5 μm size range is consistent with the idea that organic particles in this size range were adsorbed onto the soot particles, thus creating aggregation nuclei in the water column that led to the formation of very large marine aggregates. Overaggregation would have been possible because soot particles are highly surface active and have an adsorbing capacity similar to that of activated carbon [*Cornelissen et al.*, 2005; *Liang et al.*, 2006]. Such overaggregation may also have occurred as the result of soot-induced increase in TEP volume concentration. Indeed, our experimental study of the effect of soot on TEP formation showed that the input of soot in seawater strongly stimulates the formation of TEP from their dissolved precursors. Assuming that the size of the TEP pool increased in situ subsequent to soot deposition, the consequences on aggregation processes would have been twofold. First, it would have increased the overall concentration of particles and, thus, the collision frequency between particles. Second, the excess production of sticky material would have increased the overall stickiness of particles. Both mechanisms may have enhanced aggregation of particles and contributed to the observed dramatic increase of the volume concentration of particles in the surface layer.

The delay observed between the decrease in virus and DOC concentrations subsequent to soot deposition suggests that viruses could be much more reactive to soot surfaces than DOC. High adsorption rates of viruses to soot particles were reported by *Cattaneo et al.* [2010]. While this observation confirms the highly adsorptive capacity of soot, it also stresses the need to investigate the sorptive properties of soot for various solutes and particles present in the water column.

The combination of the above described soot-induced mechanism of overaggregation of small particles and the mechanism of enhanced differential sedimentation described in the previous section was likely responsible for the bimodal size distributions that occurred subsequent to deposition.

4.4. Stimulation of Microbial Processes

Both the in situ observations and the carboy experiment with soot from the Nouméa power plant showed that deposition of soot was followed by significant changes in microbial processes. The mass of soot added per liter of seawater sample in the carboy experiment (i.e., 225 to 900 μg L^{-1}) was of the same order as the increased SPM concentration measured in situ after deposition of soot-like aerosols (i.e., 450 μg L^{-1}). In both cases, the introduction of soot in seawater was followed by a decrease in abundances of free bacteria and viruses and a stimulation of activities of attached and bulk bacteria.

The twofold increase in the %BP > 1 μm and the increase of bulk BP by a factor of 3 within a week as observed in situ were higher than the weekly changes typically observed in the same environment [*Torréton et al.*, 2010] and over years at our sampling station. Indeed, the bulk BP value we observed before deposition of soot-like aerosols (i.e., 0.05 μg C L^{-1} h^{-1}) was within the range of historical values at our sampling station, where bulk BP had been determined on 12 occasions distributed over all seasons (average: 0.04 ± 0.02 μg C L^{-1} h^{-1}; range: 0.012 to 0.076 μg C L^{-1} h^{-1}; J. P. Torréton, Bacterial production, unpublished data, 1999, 2002, 2003, 2008). In addition, attached (>1 μm) BP value we observed before deposition of soot-like aerosols (i.e., 14.5% ±1.2%) was within the range of historical values at our sampling station, where %BP > 1 μm had been determined on four occasions (range: 9 to 12%; J. P. Torréton, Bacterial production > 1 μm, unpublished data, 1999). Comparison with historical data at our sampling station indicates that bacterial activity (bulk and attached) we measured before deposition of soot-like aerosols was typical for our sampling station, and the values we observed subsequent to this deposition event were remarkably high.

The increases in both %BP > 1 μm and bulk BP could be interpreted as microbial responses to deposition of soot-like aerosols. Our field observations suggest that the introduction of soot particles in the upper water column altered microbial processes, e.g., by increasing the concentration of microenvironments for microbes,

and results from the soot-enrichment carboy experiment confirmed the link between soot input in the marine system and enhanced bacterial activity. Three scenarios that are not mutually exclusive may explain the enhanced %BP > 1 μm: (1) free bacteria may have been passively adsorbed onto soot [*Cattaneo et al.*, 2010]; (2) free bacteria may have actively colonized the macroaggregates [*Kiørboe and Jackson*, 2001] resulting from soot-induced overaggregation; and (3) free bacteria might have even contributed to overaggregation by acting as nuclei [*Weinbauer et al.*, 2012]. Once associated with the newly formed microenvironments, bacteria may directly use soot and/or use organic matter concentrated on soot particles.

The close relationship between the decrease in viral abundance and the increase in SPM observed in situ is consistent with the idea of a direct adsorption of viruses onto the excess material responsible for the increase in SPM concentration. Since reference diesel soot is known to adsorb viruses very efficiently [*Weinbauer et al.*, 2009; *Cattaneo et al.*, 2010], the excess material responsible for the increase in SPM concentration is likely to be soot particles. According to this idea and to the observed relationship between concentrations of viruses (L^{-1}) and SPM ($\mu g \, L^{-1}$) in the present study (i.e., [Virus] $\sim -5 \times 10^6$ [SPM] $+ 7 \times 10^9$), an input of 1 μg of soot in seawater could have adsorbed approximately 5×10^6 viruses. Regarding free bacteria, the decrease of their abundance was not related to variation in SPM but instead to variations in particle volume concentration. Although the latter relationship is weak and must be interpreted with caution, it suggests that the observed decrease in abundance of free bacteria may not have been linked to direct adsorption onto soot, unlike viruses, but may have instead resulted from an active colonization of the large aggregates formed during soot-induced overaggregation.
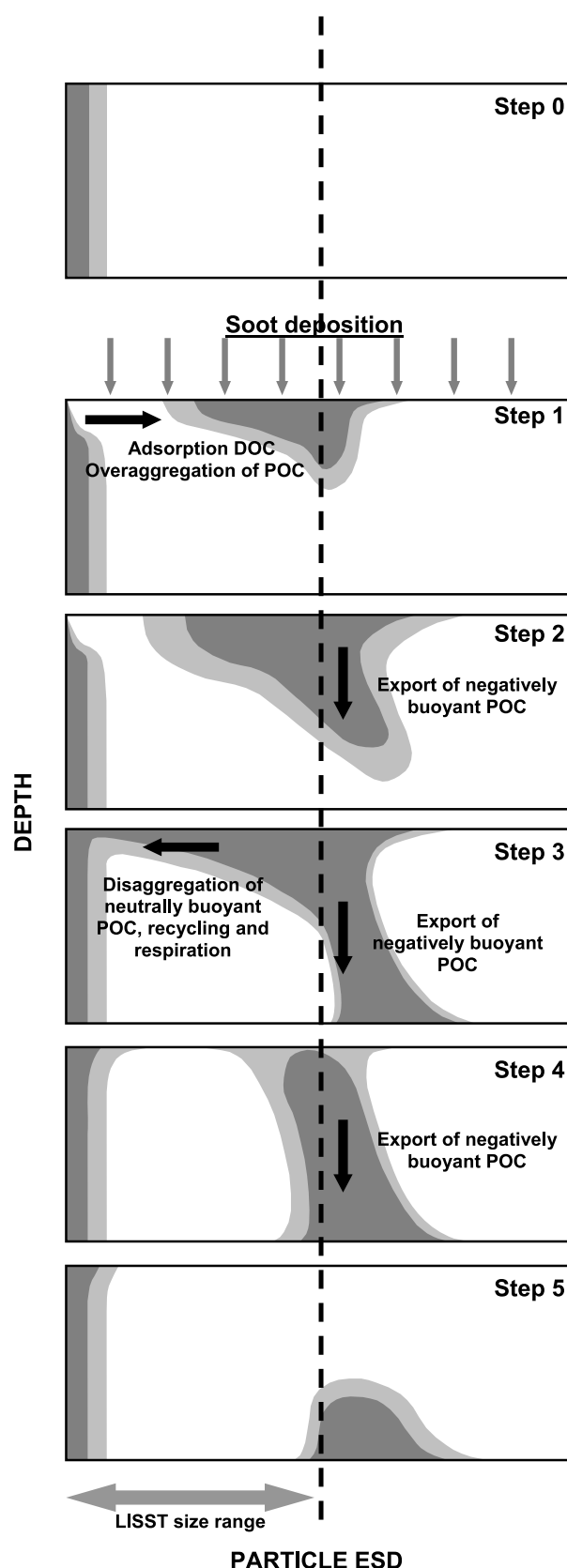
Hence, the enhanced bulk BP and %BP > 1 μm observed in situ and during the carboy experiment could be partly explained by the partial inactivation of viruses by adsorption onto soot particles, causing a decrease in virus-mediated bacterial mortality, coupled with an active bacterial colonization of more abundant microenvironments.

The observed increase in bulk BP resulted in an increase in BR and BGE. It follows that the addition of soot may have increased the length of the transit of carbon trough the bacterial pool and hence the ratio of heterotrophic respiration to primary production. This would have contributed to increase the overall heterotrophic activity of the marine ecosystem and thus its contribution of atmospheric CO_2. Finally, there was no enhancement of PP and chl *a* concentration following the input of soot-like aerosols to the system. However, the in situ observations that chl *a* concentration increased by 160% on 19 November suggest that soot deposition may have had a late, indirect effect on PP linked to enhanced bacterial remineralization resulting from the stimulation of bacterial growth.

4.5. Potential Global Effects on Ocean Ecosystems

At our sampling station, DOC concentration decreased by 3.67 μmol DOC L^{-1} from 12 to 14 November. This was the exact same period when deposition of soot-like aerosols took place (atmospheric transport and deposition model), indicating there was a link between deposition of soot-like aerosols and quantitative removal of DOC.

In addition to the quantitative removal of DOC, soot deposition may qualitatively influence the composition of the DOC pool by selectively removing the most reactive dissolved compounds, which would preferentially leave refractory DOC in solution. These reactive compounds include the high molecular weight DOC fraction, i.e., colloidal material largely composed of polysaccharides that represent up to 10–40% of DOC [*Benner et al.*, 1992]. The presence of soot material in the colloidal fraction [*Ziolkowski and Druffel*, 2010] suggests that soot may interact efficiently with high molecular weight DOC, thus favoring the transfer of colloidal soot from the dissolved to the particulate phase. Another reactive fraction of the dissolved pool is composed of persistent organic pollutants (POPs) which are known to adsorb very efficiently onto soot particles in marine environments [*Cornelissen et al.*, 2005; *Lohmann et al.*, 2005; *Persson et al.*, 2005]; this process may modify the uptake of anthropogenic pollutants by marine organisms in the water column, as demonstrated for sedimentary POPs [*Koelmans et al.*, 2006]. Amongst the potential consequences of such selective removal, one could hypothesize an accelerated scavenging of anthropogenic pollutants and a shunt of DOC from the microbial loop. Ultimately, this process may lead to an alteration of the intertwined relationship between the microbial carbon pump [*Jiao et al.*, 2010] and the biological carbon pump, by siphoning reactive organic matter out of the dissolved pool and exporting it downward.

Figure 11. Schematic representation of the five successive phases of the biogeochemical changes that follow soot deposition (explanations in the text). The position of the vertical arrows representing soot deposition at the sea surface does not relate to the size of the soot particles.

Estimates of soot emissions based on the reconstruction of fossil fuel consumption since the 1850s have showed that they have increased by a factor of ~5 during the past 150 years [*Bond et al.*, 2007]. The resulting selective removal of the soot-reactive DOC fraction may have significantly modified the composition, pathways, and spatial distributions (at the macroscales and microscales) of DOC in surface ocean waters since the beginning of the industrial revolution. Although the potential impact of soot on DOC may have been highest in western areas during the early stage of the industrial era, the effects may have switched nowadays to marine systems in the vicinity of emerging industrial countries that are mostly located in Asia [*Novakov et al.*, 2003; *Bond et al.*, 2013].

4.6. Implications and Future Prospects

Our study has shown that the effects of soot deposition on the ocean are not only limited to the enrichment of waters by the associated macronutrients and trace metals [*Luo et al.*, 2008; *Guo et al.*, 2012] but also include both a physical effect linked to the ability of soot to adsorb DOC and promote aggregation and a biological effect linked to the stimulation of bacterial activity. These effects may develop in the five-step sequence schematized in Figure 11 (step 1). Soot deposition leads to both adsorption of DOC and overaggregation of POC, which result in an increased transfer of organic matter from the dissolved to the particulate pool. The excess POC formed may (steps 2–5) sink out of the surface layer or be recycled/disrupted in surface waters. The ability of soot to stimulate a variety of carbon pathways shows that these particles may have a strong influence on the functioning of microbial pelagic systems.

The above global estimates are marked by uncertainties, which are linked to the fact that the actual mass of soot deposited on

the ocean during the present study was not available, and the potential variations of soot-sorptive properties as a function of soot sources and composition are not known. Even with these uncertainties, it is obvious that the introduction of soot in the water column may have significant effects on ocean surface particles, DOC dynamics, and microbial processes and that these effects are expected to be highest in the tropical belt and in the Northern Hemisphere in agreement with the global emission and deposition patterns of soot [*Liousse et al.*, 1996; *Loescher et al.*, 2004; *Jurado et al.*, 2008; *Bond et al.*, 2013], especially in waters near emission hot spots. This stresses the need for investigations dedicated to the effects of soot on pelagic systems, which are presently poorly documented.

References

Ahlberg, M., L. Berghem, G. Nordberg, S.-A. Persson, L. Rudling, and B. Steen (1983), Chemical and biological characterization of emissions from coal- and oil-fired power plants, *Environ. Health Perspect.*, *47*, 85–102.

Benner, R., J. D. Pakulski, M. McCarthy, J. I. Hedges, and P. G. Hatcher (1992), Bulk chemical characteristics of dissolved organic matter in the ocean, *Science*, *255*, 1561–1564.

Bond, T. C., D. G. Streets, K. F. Yarber, S. M. Nelson, J.-H. Woo, and Z. Klimont (2004), A technology-based global inventory of black and organic carbon emissions from combustion, *J. Geophys. Res.*, *109*, D14203, doi:10.1029/2003JD003697.

Bond, T. C., E. Bhardwaj, R. Dong, R. Jogani, S. Jung, C. Roden, D. G. Streets, and N. M. Trautmann (2007), Historical emissions of black and organic carbon aerosol from energy-related combustion, 1850–2000, *Global Biogeochem. Cycles*, *21*, GB2018, doi:10.1029/2006GB002840.

Bond, T. C., et al. (2013), Bounding the role of black carbon in the climate system: A scientific assessment, *J. Geophys. Res. Atmos.*, *118*, 5380–5552, doi:10.1002/jgrd.50171.

Cachier, H., M. P. Bremond, and P. Buat-Menard (1989), Determination of atmospheric soot carbon with a simple thermal method, *Tellus, Ser. B*, *41*, 379–390.

Cattaneo, R., C. Rouvière, F. Rassoulzadegan, and M. G. Weinbauer (2010), Association of marine viral and bacterial communities with reference black carbon particles under experimental conditions: An analysis with scanning electron, epifluorescence and confocal laser scanning microscopy, *FEMS Microbiol. Ecol.*, *74*(2), 382–396.

Chen, F., J. R. Lu, B. J. Binder, Y. C. Liu, and R. E. Hodson (2001), Application of digital image analysis and flow cytometry to enumerate marine viruses stained with SYBR gold, *Appl. Environ. Microbiol.*, *67*, 539–545.

Choi, M. Y., G. W. Mulholland, A. Hamins, and T. Kashiwagi (1995), Comparisons of the soot volume fraction using gravimetric and light extinction techniques, *Combust. Flame*, *102*(1–2), 161–169.

Chung, C. E., V. Ramanathan, D. Kim, and I. A. Podgorny (2005), Global anthropogenic aerosol direct forcing derived from satellite and ground-based observations, *J. Geophys. Res.*, *110*, D24207, doi:10.1029/2005JD00635.

Cornelissen, G., Ö. Gustafsson, T. D. Bucheli, M. T. Jonker, A. A. Koelmans, and P. C. M. van Noort (2005), Extensive sorption of organic compounds to black carbon, coal, and kerogen in sediments and soils: Mechanisms and consequences for distribution, *Environ. Sci. Technol.*, *39*, 6881–6895.

Dachs, J., and S. J. Eisenreich (2000), Adsorption onto aerosol soot carbon dominates gas-particle partitioning of polycyclic aromatic hydrocarbons, *Environ. Sci. Technol.*, *34*, 3690–3697.

del Giorgio, P. A., and J. J. Cole (1998), Bacterial growth efficiency in natural aquatic systems, *Annu. Rev. Ecol. Syst.*, *29*, 503–541.

Dittmar, T., and B. P. Koch (2006), Thermogenic organic matter dissolved in the abyssal ocean, *Mar. Chem.*, *102*, 208–217.

Dittmar, T., and J. Paeng (2009), A heat-induced molecular signature in marine dissolved organic matter, *Nat. Geosci.*, *2*(3), 175–179.

Dittmar, T., J. Paeng, T. M. Gihring, I. G. N. A. Suryaputra, and M. Huettel (2012), Discharge of dissolved black carbon from a fire-affected intertidal system, *Limnol. Oceanogr.*, *57*(4), 1171–1181.

Fast, J. D., and R. C. Easter (2006), A LaGrange particle dispersion model compatible with WRF 7th WRF Users' Workshop, National Center for Atmospheric Research, June 19–22, Boulder, Colo., p. 6.2.

Flores-Cervantes, D. X., D. L. Plata, J. K. MacFarlane, C. M. Reddy, and P. M. Gschwend (2009), Black carbon in marine particulate organic carbon: Inputs and cycling of highly recalcitrant organic carbon in the Gulf of Maine, *Mar. Chem.*, *113*, 172–181.

Guo, C., J. Yu, T.-Y. Ho, L. Wang, S. Song, L. Kong, and H. Liu (2012), Dynamics of phytoplankton community structure in the South China Sea in response to the East Asian aerosol input, *Biogeosciences*, *9*, 1519–1536.

Gustafsson, Ö., F. Haghseta, C. Chan, J. MacFarlane, and P. M. Gschwend (1997), Quantification of the dilute sedimentary soot phase: Implications for PAH speciation and bioavailability, *Environ. Sci. Technol.*, *31*(1), 203–209.

Gustafsson, Ö., T. Bucheli, Z. Kukulska, M. Andersson, C. Largeau, J.-N. Rouzaud, C. Redd, and T. Eglinton (2001), Evaluation of a protocol for the quantification of black carbon in sediments, *Global Biogeochem. Cycles*, *15*, 881–890, doi:10.1029/2000GB001380.

Hadley, O. L., V. Ramanathan, G. R. Carmichael, Y. Tang, C. E. Corrigan, G. C. Roberts, and G. S. Mauger (2007), Trans-Pacific transport of black carbon and fine aerosols (D < 2.5 μm) into North America, *J. Geophys. Res.*, *112*, D05309, doi:10.1029/2006JD007632.

Holm-Hansen, O., C. J. Lorenzen, R. W. Holmes, and J. D. H. Strickland (1965), Fluorimetric determination of chlorophyll, *Rapp. P. V. Reun. Cons. Int. Explor. Mer.*, *30*, 3–15.

Jacobson, M. Z. (2002), Control of fossil-fuel particulate black carbon plus organic matter, possibly the most effective method of slowing global warming, *J. Geophys. Res.*, *107*(D19), 4410, doi:10.1029/2001JD001376.

Jiao, N., et al. (2010), The microbial carbon pump in the ocean, *Nat. Rev. Microbiol.*, *8*, 593–599.

Jouon, A., P. Douillet, S. Ouillon, and P. Fraunié (2006), Calculations of hydrodynamic time parameters in a semi-opened coastal zone using a 3D hydrodynamic model, *Cont. Shelf Res.*, *26*, 1395–1415.

Junker, C., and C. A. Liousse (2006), Global emission inventory of carbonaceous aerosol from historic records of fossil fuel and biofuel consumption for the period 1860–1997, *Atmos. Chem. Phys. Discuss.*, *6*, 4897–4927.

Jurado, E., J. Dachs, C. M. Duarte, and R. Simóc (2008), Atmospheric deposition of organic and black carbon to the global oceans, *Atmos. Environ.*, *42*, 7931–7939.

Kiørboe, T., and G. A. Jackson (2001), Marine snow, organic solute plumes, and optimal chemosensory behavior of bacteria, *Limnol. Oceanogr.*, *46*, 1309–1318.

Koelmans, A. A., M. T. Jonker, G. Cornelissen, T. D. Bucheli, P. C. Van Noort, and Ö. Gustafsson (2006), Black carbon: The reverse of its dark side, *Chemosphere*, *63*, 365–377.

Kuhlbusch, T. A. J. (1995), Method for determining black carbon in residues of vegetation fires, *Environ. Sci. Technol.*, *29*(10), 1695–2702.

Lefèvre, J., P. Marchesiello, N. Jourdain, C. Menkes, and A. Leroy (2010), Weather regimes and orographic circulation around New Caledonia, *Mar. Pollut. Bull.*, *61*, 413–431.

Liang, B., et al. (2006), Black Carbon increases cation exchange capacity in soils, *Soil Sci. Soc. Am. J.*, *70*, 1719–1730.

Liousse, C., J. E. Penner, C. Chuang, J. J. Walton, H. Eddleman, and H. Cachier (1996), A global three-dimensional model study of carbonaceous aerosols, *J. Geophys. Res.*, *101*, 19,411–19,432, doi:10.1029/95JD03426.

Loescher, H. W., J. A. Bentz, S. F. Oberbauer, T. K. Ghosh, R. V. Tompson, and S. K. Loyalka (2004), Characterization and dry deposition of carbonaceous aerosols in a wet tropical forest canopy, *J. Geophys. Res.*, *109*, D02309, doi:10.1029/2002JD003353.

Lohmann, R., J. K. MacFarlane, and P. M. Gschwend (2005), Importance of black carbon to sorption of native PAHs, PCBs, and PCDDs in Boston and New York, Harbor sediments, *Environ. Sci. Technol.*, *39*, 141–148.

Lohmann, R., K. Bollinger, M. Cantwell, J. Feichter, I. Fischer-Bruns, and M. Zabel (2009), Fluxes of soot black carbon to South Atlantic sediments, *Global Biogeochem. Cycles*, *23*, GB1015, doi:10.1029/2008GB003253.

Luo, C., N. Mahowald, T. Bond, P. Y. Chuang, P. Artaxo, R. Siefert, Y. Chen, and J. Schauer (2008), Combustion iron distribution and deposition, *Global Biogeochem. Cycles*, *22*, GB1012, doi:10.1029/2007GB002964.

Mannino, A., and H. Harvey (2004), Black carbon in estuarine and coastal ocean dissolved organic matter, *Limnol. Oceanogr.*, *49*, 735–740.

Marañón, E., P. Cermeño, E. Fernández, J. Rodríguez, and L. Zabala (2004), Significance and mechanisms of photosynthetic production of dissolved organic carbon in a coastal eutrophic ecosystem, *Limnol. Oceanogr.*, *49*, 1652–1666.

Marchesiello, P., J. Lefèvre, A. Vega, X. Couvelard, and C. Menkès (2010), Coastal upwelling, circulation and heat balance around New Caledonia's barrier reef, *Mar. Pollut. Bull.*, *61*, 432–448.

Mari, X. (1999), Carbon content and C:N ratio of transparent exopolymeric particles (TEP) produced by bubbling exudates of diatoms, *Mar. Ecol. Prog. Ser.*, *183*, 59–71.

Mari, X., and A. B. Burd (1998), Seasonal size spectra of transparent exopolymeric particles (TEP) in a coastal sea and comparison with those predicted using coagulation theory, *Mar. Ecol. Prog. Ser.*, *163*, 63–76.

Mari, X., and M. Robert (2008), Metal induced variations of TEP sticking properties in the southwestern lagoon of New Caledonia, *Mar. Chem.*, *110*, 98–108.

Masiello, C. A., and E. R. M. Druffel (1998), Black carbon in deep-sea sediments, *Science*, *280*, 1911–1913.

McCave, I. N. (1984), Size spectra and aggregation of suspended particles in the deep ocean, *Deep Sea Res.*, *31*, 329–352.

Middelburg, J. J., J. Nieuwenhuize, and P. van Breugel (1999), Black carbon in marine sediments, *Mar. Chem.*, *65*, 245–252.

Mitra, S., T. S. Bianchi, B. A. McKee, and M. Sutula (2002), Black carbon from the Mississippi River: Quantities, sources, and potential implications for the global carbon cycle, *Environ. Sci. Technol.*, *36*, 2296–2302.

Nguyen, T. H., R. A. Brown, and W. P. Ball (2004), An evaluation of thermal resistance as a measure of black carbon content in diesel soot, wood char, and sediment, *Org. Geochem.*, *35*, 217–234.

Novakov, T., V. Ramanathan, J. E. Hansen, T. W. Kirchstetter, M. Sato, J. E. Sinton, and J. A. Sathaye (2003), Large historical changes of fossil-fuel black carbon aerosols, *Geophys. Res. Lett.*, *30*(6), 1324, doi:10.1029/2002GL016345.

Ogren, J. A., and R. J. Charlson (1983), Elemental carbon in the atmosphere: Cycle and lifetime, *Tellus, Ser. B*, *35*, 241–254.

Passow, U., and A. L. Alldredge (1994), Distribution, size and bacterial colonization of transparent exopolymer particles (TEP) in the ocean, *Mar. Ecol. Prog. Ser.*, *113*, 185–198.

Persson, N. J., Ö. Gustafsson, T. D. Bucheli, R. Ishaq, K. Næs, and D. Broman (2005), Distribution of PCNs, PCBs, and other POPs together with soot and other organic matter in the marine environment of the Grenlandsfjords, Norway, *Chemosphere*, *60*, 274–283.

Raimbault, P., N. Garcia, and F. Cerutti (2008), Distribution of inorganic and organic nutrients in the South Pacific Ocean—Evidence for long-term accumulation of organic matter in nitrogen depleted waters, *Biogeosciences*, *5*, 281–298.

Ramanathan, V., and G. Carmichael (2008), Global and regional climate changes due to black carbon, *Nat. Geosci.*, *1*, 221–227.

Ramanathan, V., et al. (2007), Atmospheric brown clouds: Hemispherical and regional variations in long range transport, absorption and radiative forcing, *J. Geophys. Res.*, *112*, D22S21, doi:10.1029/2006JD008124.

Rochelle-Newall, E. J., J.-P. Torréton, X. Mari, and O. Pringault (2008), Phytoplankton-bacterioplankton coupling in a subtropical South Pacific coral reef lagoon, *Aquat. Microb. Ecol.*, *50*, 221–229.

Shindell, D., and G. Faluvegi (2009), Climate response to regional radiative forcing during the twentieth century, *Nat. Geosci.*, *2*, 294–300.

Smith, D. C., and F. Azam (1992), A simple, economical method for measuring bacterial protein synthesis rates in seawater using ³H-leucine, *Mar. Microb. Food Webs*, *6*, 107–114.

Song, J., and P. Peng (2010), Characterisation of black carbon materials by pyrolysis–gas chromatography–mass spectrometry, *J. Anal. Appl. Pyrolysis*, *87*, 129–137.

Torréton, J.-P., E. J. Rochelle-Newall, O. Pringault, S. Jacquet, V. Faure, and E. Briand (2010), Variability of primary and bacterial production in a coral reef lagoon (New Caledonia), *Mar. Pollut. Bull.*, *61*, 335–348.

Vignati, E., M. Karl, M. Krol, J. Wilson, P. Stier, and F. Cavalli (2010), Sources of uncertainties in modelling black carbon at the global scale, *Atmos. Chem. Phys.*, *10*, 2595–2611.

Weinbauer, M. G., Y. Bettarel, R. Cattaneo, B. Luef, C. Maier, C. Motegi, P. Peduzzi, and X. Mari (2009), Viral ecology of organic and inorganic particles in aquatic systems: Avenues for future research, *Aquat. Microb. Ecol.*, *57*, 321–341.

Weinbauer, M. G., R. Cattaneo, J. M. Gasol, J. G. Herndl, X. Mari, C. Migon, and F. Rassoulzadegan (2012), Black carbon and microorganisms in aquatic systems, in *Advances in Environmental Research*, vol. 25, edited by J. A. Daniels, pp. 1–37, Nova Publishers, New York.

Ziolkowski, L. A., and E. R. M. Druffel (2010), Aged black carbon identified in marine dissolved organic carbon, *Geophys. Res. Lett.*, *37*, L16601, doi:10.1029/2010GL043963.